Mixed valence Sn doped $(CH_3NH_3)_3Bi_2Br_9$ produced by mechanochemical synthesis

Xiaohan Jia,[1] Yuhan Liu,[1,2] Robin S. Perry,[2,3] Ivan P. Parkin,[1] Robert G. Palgrave[1]*

1. Department of Chemistry, University College London, 20 Gordon Street, London, WC1H 0AJ

2. London Centre for Nanotechnology and Department of Physics and Astronomy, University College London, London WC1E 6BT, United Kingdom

3. ISIS neutron spallation source, Rutherford Appleton Laboratory (RAL), Harwell Campus, Didcot OX11 0QX, United Kingdom

Abstract

Bismuth halides with formula $A_3Bi_2X_9$, where A is an inorganic or organic cation, show desirable properties as solar absorbers and luminescent materials. Control of structural and electronic dimensionality of these compounds is important to yield materials with good light absorption and charge transport. Here we report mechanochemical reaction of $(CH_3NH_3)_3Bi_2Br_9$ with $SnBr_2$ at room temperature in air, yielding a material with strong absorption across the visible and near-infrared (NIR) region. We attribute this to mixed valence doping of Sn(II) and Sn(IV) on the Bi site. X-ray diffraction shows no secondary phases, even after heating at 200°C to improve crystallinity. X-ray photoelectron spectroscopy suggests the presence of Sn(II) and Sn(IV) states. A similar approach to dope Sn into the iodide analogue $(CH_3NH_3)_3Bi_2I_9$ was unsuccessful.

Introduction

Halide perovskites with formula ABX_3, where A and B are cations, X is halide, have recently been found as desirable solar absorbers.[1-3] Compared with the most widely commercialised silicon solar cell, solution-processable halide perovskite solar cells have several advantages, including high optical absorption coefficient, defect tolerance, and tunable band gap.[4] However, the most commonly used B-site metal, Pb, hinders commercialisation due to the high toxicity and the poor intrinsic air stability of many Pb(II) based perovskites.[5] Thus there is motivation to develop lead-free analogues. Bi(III) shares the same electronic configuration ([Xe] $4f^{14}$ $5d^{10}$ $6s^2$) with Pb(II), and shows excellent potential as a Pb alternative: it has low toxicity, and complex bismuth halides are characterised by good air stability.[6-10] Bi(III) cannot fit into the ABX_3 perovskite structure, but instead forms a series of structures with distorted BiX_6 corner-or-edge-shared octahedra, leading to halide perovskite derivatives, $A_3Bi_2X_9$ which adopt either 0D, 1D or 2D inorganic sublattices.[11-14] The 2D layered structure is of special interest due to its vibronic properties and electronic strucutre,[15, 16] and remarkable luminescent efficiencies.[14] The 2D structure is formed when X is bromide ion, while when X is iodide, the material

adopts a 0D structure, with isolated $[Bi_2I_9]^{3-}$ clusters. While the use of iodide anions results in greater light absorption due to a smaller band gap, the 0D iodide structure is detrimental to carrier mobility. Likewise, the 2D $A_3Bi_2Br_9$ may show higher mobility, but suffers from relatively large bandgap energies, which limit power conversion efficiency (PCE) of photovoltaic (PV) applications.[17, 18] Here we seek to find new methods to induce visible light absorption in 2D $A_3Bi_2Br_9$ compounds, which may enhance PV properties, and also give greater control over their luminescent properties,[19] or make them suitable for other optoelectronic applications.

Intervalence charge transfer (IVCT) is defined by the electron transfer between two atoms of the same element that in the ground state have different oxidation states.[20] IVCT is known for Sb(III) / Sb(V) as well as Sn(II)/Sn(IV) in halide materials.[21] Although Sn(II) is a promising B-site candidate for lead-free perovskite solar absorber, its PV application is limited by the potential degradation of devices caused by the rapid oxidation of Sn(II) to Sn(IV).[22] Where both Sn(II) and Sn(IV) are present in the same compound, light absorption may induce electron transfer between the two sites of different oxidation state. The activation energy of the transition between the symmetrical ground states typically lies in the visible and NIR regions in the electromagnetic spectrum, and so can cause a broad and intense optical absorption peak.[23]

We have recently shown that $Cs_3Bi_2Br_9$ can be doped with mixed valence Sn through a solution phase synthesis.[24] Here we show that a related hybrid material, $MA_3Bi_2Br_9$ (MA = $(CH_3NH_3)^+$) can similarly be doped with mixed valence Sn(II) / Sn(IV) by a very rapid room temperature, solvent free mechanochemical reaction carried out in air. Mechanochemical reactions have been used as a synthesis strategy for a long time in many areas such as to prepare polymeric materials,[25] metal organic frameworks (MOFs)[26, 27] and halide perovskites.[28] Solvent-free mechanochemical reactions conducted by solid-state grinding, can be a sustainable synthesis approach.[29, 30] Here we report an ambient condition mechanochemical synthesis of a mixed valence compound, Sn: $MA_3Bi_2Br_9$. We find that partial substitution of Bi(III) with equal amounts of Sn(II) and Sn(IV) dramatically increases the optical absorption in the visible and near IR region, which corresponds to the spontaneous colour change from yellow to black during the reaction. This may be a viable strategy for overcoming the principal challenge of such 2D $A_3B_2X_9$ compounds, their large direct bandgaps (E_g = 2.6 eV for $MA_3Bi_2Br_9$).

Experimental Section

Bismuth(III) oxide (Bi_2O_3, Fine Chemicals), caesium carbonate ($Cs_2(CO)_3$, 99%, Sigma-Aldrich), hydrobromic acid (HBr, 47 wt. % in H_2O , Sigma-Aldrich), hydroiodic acid (HI, 57 wt. % in H_2O, Sigma-Aldrich), methylamine solution (CH_5N, 40 wt. % in H_2O, Sigma-Aldrich), tin(II) bromide ($SnBr_2$, Sigma-Aldrich), tin(IV) bromide ($SnBr_4$, Sigma-Aldrich), tin(II) iodide (SnI_2, 99.99%, Sigma-Aldrich), tin(II) oxide (SnO, 99%, Sigma-Aldrich) were used as received without purification.

Synthesis of $MA_3Bi_2X_9$ (MA = $CH_3NH_3^+$, X = Br or I) microcrystals

Microcrystalline $MA_3Bi_2X_9$ was synthesised by firstly reacting the stoichiometric ratio of Bi_2O_3 and aqueous methylamine separately with excess 3 M hydrobromic acid, then mixing the two solutions. For example, to prepare 5 g of $MA_3Bi_2Br_9$, pale yellow bismuth oxide powder (1.893 g, 4.26 mmol) was stirred and slowly dissolved in excess dilute hydrobromic acid (~3 M, 23 mL) at 80 °C for 10 mins to prepare the bismuth bromide precursor solution. Methylamine solution 40 wt. % in H_2O (0.989 g, MA:Bi = 3:2), was added dropwise into the bismuth bromide solution in air. The clear reaction mixture was stirred at 80 °C for another 10 mins to ensure the reaction to be completed. The bright yellow microcrystalline solid was precipitated by evaporating the solvent until sufficient product has crystallised, at which point it was isolated by filtration and dried at 60 °C in air.

Synthesis of B-site Sn doped $MA_3Bi_2Br_9$ by mechanochemical reaction

B-site mixed-valent Sn(II) / Sn(IV) doped $MA_3Bi_2Br_9$ microcrystals ($MA_3(Sn_xBi_{(1-x)})_2Br_9$) were prepared by mechanochemical reaction (solid-state grinding) at room temperature in air from stoichiometric amounts of $SnBr_2$ and the as-made $MA_3Bi_2X_9$ microcrystals.

For example, 30% Sn-doped $MA_3Bi_2Br_9$ ($MA_3(Sn_{0.3}Bi_{0.70})_2Br_9$) was prepared by grinding $SnBr_2$ powder (3 mmol) together with the as-synthesised yellow crystalline $MA_3Bi_2Br_9$ (3.5 mmol) in an agate mortar until two solids were homogeneously mixed. No solvent was added to the reaction. The colour of the reactants turned black immediately upon grinding. Samples were made with Sn contents of x = 0, 0.01, 0.25, 0.3, 0.35, 0.4, 0.5, 0.6. All samples were stored in glass sample vials in air.

To further improve homogeneity of dopant and introduce crystallinity, half of each as-synthesised $MA_3(Sn_xBi_{(1-x)})_2Br_9$ sample (including x=0, $MA_3Bi_2Br_9$) were heated at 200 °C in furnace in air for two hours.

Characterisation details are given in the Electronic Supporting Information.

Results

Yellow $MA_3Bi_2Br_9$ microcrystals showed a powder diffraction pattern matching that reported by Ishihara *et al.*,[31] and corresponding to a trigonal crystal structure with the space group *P-3m1*. Further crystallisation of as-synthesised $MA_3Bi_2Br_9$ was induced by heating at 200 °C in air, as shown by changes to the PXRD pattern (red) improved signal to noise ratio, given the same data collection parameters, in Figure 1. The preserved peak width and position in PXRD suggests no decomposition occurred, and that the crystal structure of $MA_3Bi_2Br_9$ remained unchanged, with no additional peaks appearing that might indicate decomposition.

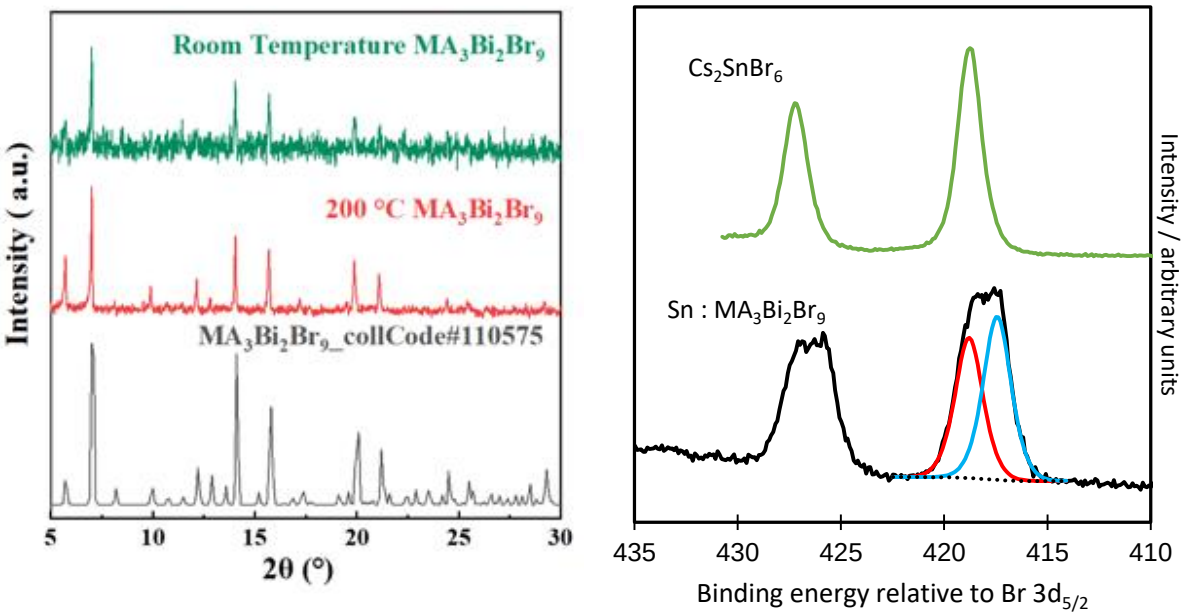

Figure 1 Left, powder XRD patterns of $MA_3Bi_2Br_9$ prepared at room temperature as-synthesised (green) and by 200 °C heating (red) in air, standard pattern from Ishihara *et al.*[31] obtained from ICSD database (black). Right Sn 3d XPS of Sn : $MA_3Bi_2Br_9$ freshly produced by mechanical grinding of $MA_3Bi_2Br_9$ and $SnBr_2$, as well as Cs_2SnBr_6 as a reference compound. Note that the binding energy scale is shown relative to Br $3d_{5/2}$ as discussed in the text.

During room temperature mechanochemical reactions between microcrystalline $MA_3Bi_2Br_9$ and $SnBr_2$, a rapid colour change from bright yellow to black began to occur as soon as the two solids came into contact, and proceeded rapidly upon grinding to give a homogenous colour change after less than one minute (Figure 2). In contrast, no obvious colour change occurred when $MA_3Bi_2Br_9$ was ground with $SnBr_4$ instead of $SnBr_2$. The powder XRD patterns of different Sn-content, mechanochemically doped $MA_3(Sn_xBi_{(1-x)})_2Br_9$ samples (where x = 0, 0.01, 0.25, 0.3, 0.35, 0.4, 0.5, 0.6) are presented in Figure 2. No secondary phase of potential impurities, including starting material $SnBr_2$, or possible by-products $BiBr_3$ or MA_2SnBr_6 is seen. For Sn-doped materials, diffraction peaks remained at the same position

compared with undoped $MA_3Bi_2Br_9$ indicating no detectable change in lattice parameters. The peak widths were slightly broadened with the increasing amount of Sn added, indicating some disorder, strain, or reduction in crystallite size upon doping. The disappearance of reactant $SnBr_2$, which is not detected in PXRD of the product, and the colour change of the reaction mixture both indicated that a reaction had occurred.

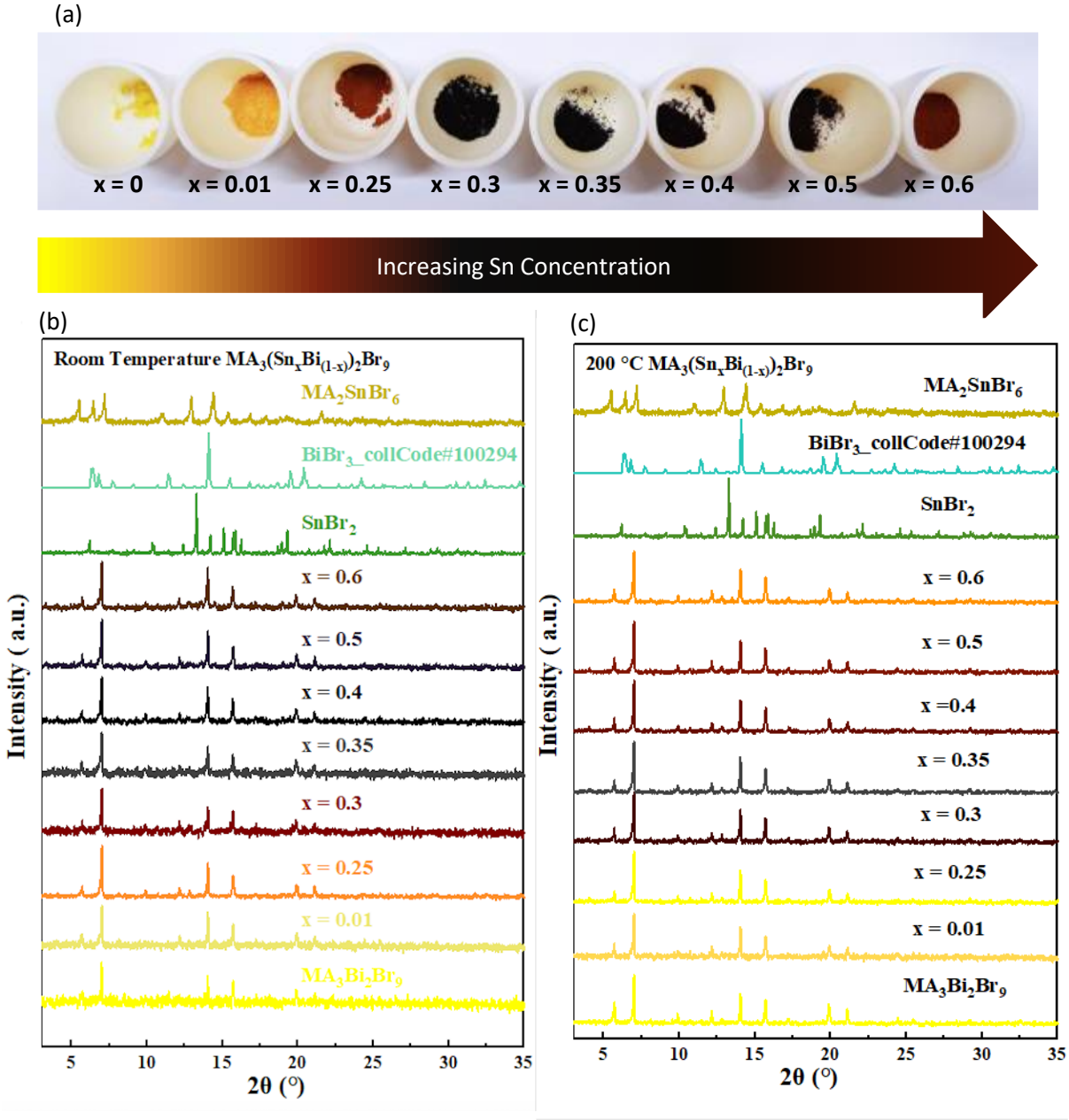

Figure 2 (a) Sample colour changes with Sn content for $MA_3(Sn_xBi_{(1-x)})_2Br_9$ **(b)** and **(c)** Powder XRD patterns of room-temperature and 200°C heated $MA_3(Sn_xBi_{(1-x)})_2Br_9$ microcrystal together with the patterns of dopant material $SnBr_2$, potential by-products of $BiBr_3$, MA_2SnBr_6.

All as-synthesised $MA_3(Sn_xBi_{(1-x)})_2Br_9$ samples were heated at 200 °C in air for 2 hours to enhance crystallinity and homogeneity, and the PXRD patterns are shown in Figure 2. The greater signal to noise ratio in the PXRD data collected with the same acquisition parameters suggests greater crystallinity in the annealed samples. No additional diffraction peaks are seen after annealing, showing the stability of the doped material under the annealing conditions.

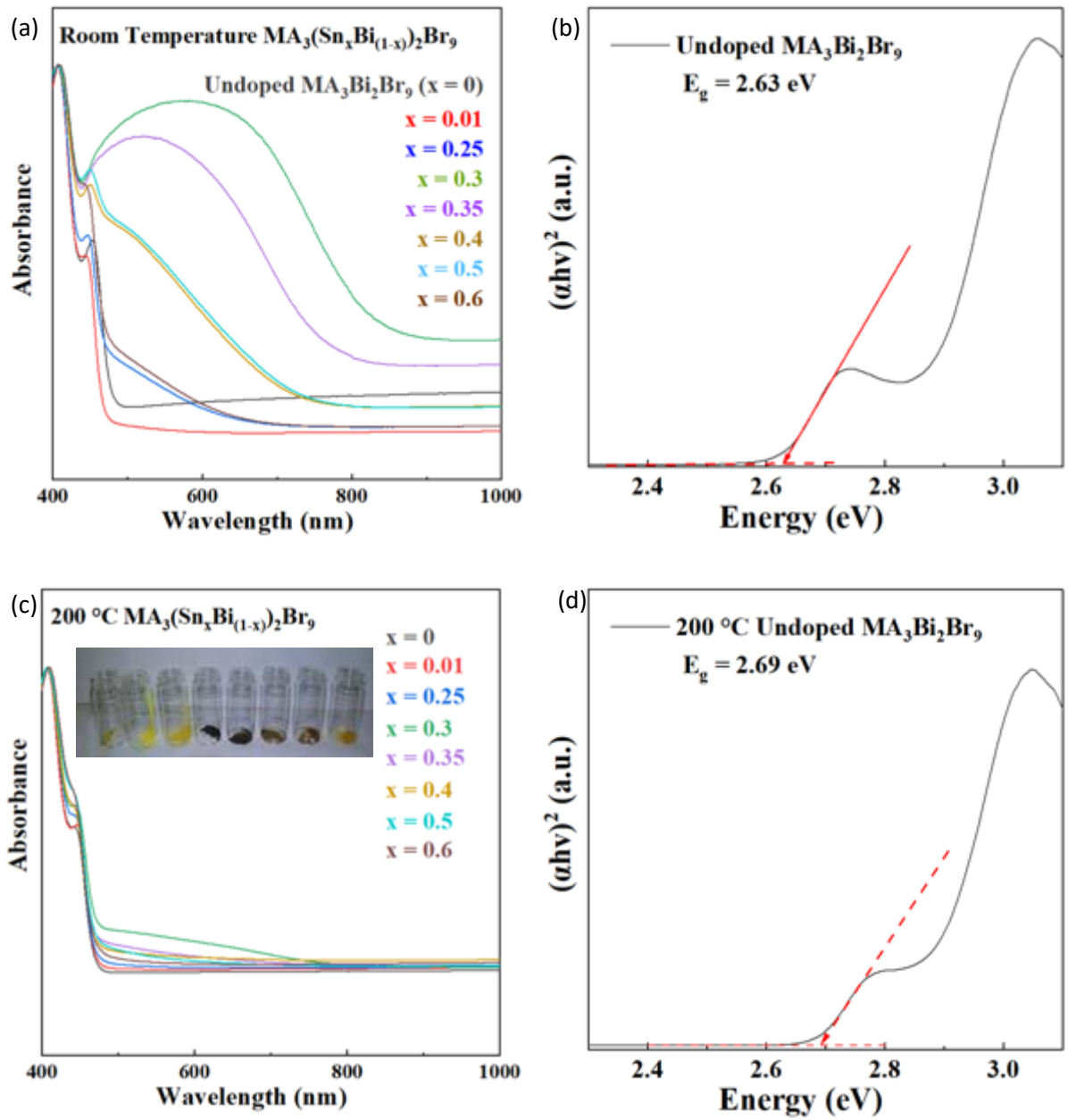

Figure 3 (a) UV-Vis absorbance spectra of room temperature doped $MA_3(Sn_xBi_{(1-x)})_2Br_9$. **(b)** Demonstration of bandgap energy calculation from Tauc-analysis. **(c)** UV-Vis absorbance spectra of 200 °C heated $MA_3(Sn_xBi_{(1-x)})_2Br_9$, insert shows the colours of 200 °C heated $MA_3(Sn_xBi_{(1-x)})_2Br_9$ samples, from left to right x = 0, 0.01, 0.25, 0.3, 0.35, 0.4, 0.5, 0.6. **(d)** Example calculation of the bandgap energy of 200 °C heated undoped $MA_3Bi_2Br_9$ from Tauc-analysis.

The UV-Vis absorbance spectra of room temperature mechanochemically doped $MA_3(Sn_xBi_{(1-x)})_2Br_9$, taken from diffuse reflectance measurements using the Kubelka Munk function, is shown in Figure 3a. The broad absorption peaks present in the visible and near infra red regions in Sn-doped microcrystals show significant enhancement of light absorbance in our doped materials. This enhancement was greatest at x = 0.3, 0.35, corresponding to the greatest colour changes of as-synthesised materials.

XPS was used to probe the composition and chemical environments of Sn in the doped system. The additional Sn peaks in XPS survey spectra for $MA_3(Sn_xBi_{(1-x)})_2Br_9$ compared with pure phase $MA_3Bi_2Br_9$ shows that Sn was successfully detected in all doped samples. Survey spectra of the selected $MA_3(Sn_x$-$Bi_{(1-x)})_2Br_9$ before and after heating are presented in S3. No additional unexpected element except O was detected. The oxygen can be associated with by-products of oxides or oxyhalides such as BiOBr, although none were detected from XRD, which may be due to limited crystallinity.

The analytical ratio of Sn to Bi for each sample was calculated from the average of three XPS measurements by applying the equation $\frac{[Sn]}{[Sn]+[Br]} \times 100\%$ (Table 1). For room temperature synthesised compounds, XPS values were within ±10 atomic % of nominal amounts, and the absolute errors between repeat measurements were ±5 atomic %. The surface sensitive nature of XPS may be the cause of the discrepancy with nominal values if the surface has a different composition to the bulk. For the heated samples, except for x = 0.30, all samples have the percentage error within ±2% to the theoretical ratios. This suggests that by annealing, the homogeneity of doped materials can be successfully increased.

The Sn 3d spectra from $MA_3(Sn_xBi_{(1-x)})_2Br_9$ are shown in Figure 1. In common with other post transition metals, determination of Sn oxidation state by XPS can be challenging. An additional complication faced here is that binding energies are often referenced to adventitious C1s peaks. This approach has faced recent criticism,[32, 33] and is especially difficult to implement in this case as our compounds contain carbon in the MA^+ cation. Therefore to understand the x-ray photoemission spectra were taken from $MA_3(Sn_xBi_{(1-x)})_2Br_9$, and Cs_2SnBr_6, the latter a compound nominally containing only Sn(IV) which was synthesised as described previously.[34] To avoid the need to calibrate the binding energy scale using C 1s, we measured the difference in energy between the Sn $3d_{5/2}$ and Br $3d_{5/2}$ peaks, which are present in both Cs_2SnBr_6 and $MA_3(Sn_xBi_{(1-x)})_2Br_9$. With the assumption that the bromide anion does not significantly change chemical environment in these compounds, the binding energy difference between Sn 3d and Br 3d can be interpreted as due to a change in the chemical environment of Sn. To obtain the Br $3d_{5/2}$ binding energy, the Br 3d spectrum was modelled with two components which had their binding energy separation and relative area constrained to literature values, and which were of equal FWHM and lineshape. The Sn 3d spin orbit doublet is well separated, so no deconvolution of the $3d_{5/2}$ and $3d_{3/2}$ was necessary. The Sn $3d_{5/2}$ peak was found to be well modelled by a single Gaussian-Lorentzian peak over a Shirley background for Cs_2SnBr_6. The FWHM of the Sn $3d_{5/2}$ peak in Cs_2SnBr_6 was 1.38 eV. The energy difference between the Sn $3d_{5/2}$ and the Br $3d_{5/2}$ peaks for Cs_2SnBr_6 418.8 eV. In Sn : $MA_3Bi_2Br_9$, the $Sn3d_{5/2}$ spectrum consists of two maxima, and can be modelled well with two Gaussian Lorentzian components. By constraining the FWHM and lineshape to be equal, the

best fit sees components at binding energies of 489.6 eV and 488.2 eV and each with FWHM 1.66 eV. Since the Br $3d_{5/2}$ binding energy in $MA_3(Sn_xBi_{(1-x)})_2Br_9$ is 70.8 eV, the Sn3d-Br3d energy differences are 418.8 eV and 417.4. Thus the higher binding energy Sn 3d component in Sn : $MA_3Bi_2Br_9$ has the same energy relative to Br 3d as found in Cs_2SnBr_6; we assign this as a Sn(IV) component. The lower binding energy component is assigned as a Sn(II) environment. Attempts to further confirm this assignment, by measuring a Sn(II) standard such as $SnBr_2$ were hampered by oxidation on the surfaces of samples of $SnBr_2$ available to us. The Sn(IV) : Sn(II) ratio from this analysis was 0.86 : 1, showing there is a slight excess of Sn(II) compared to the expected case of equal quantities of Sn(IV) and Sn(II). We attribute the emerging of the broad optical absorption peaks seen in Figure 3 to the presence of IVCT resulting from the introduction of mixed-valence Sn(II) and Sn(IV).

The Tauc method[35] gives the direct bandgap energy of $MA_3Bi_2Br_9$ as E_g = 2.63 eV, which matches well with the report of Qi *et al.* (who found a bandgap of 2.65 eV),[36] but Leng *et al.* found a bandgap of 2.5 eV for single crystals.[19] The band gap energies of $MA_3(Sn_xBi_{(1-x)})_2Br_9$ could not be measured in the same way due to the strong IVCT absorption which obscures the band edge. The annealed $MA_3(Sn_xBi_{(1-x)})_2Br_9$ microcrystals, possess the same general trend in terms of sample colour and absorption enhancement in the visible and NIR regions as shown in Figure 3a. From the spectra, it is clear that the interband transition is much more intense than the IVCT absorption in the annealed samples, likely due to increased crystallinity. We notice that the macroscopic appearance of majority heated $MA_3(Sn_xBi_{(1-x)})_2Br_9$ samples remained as deep coloured, especially for x = 0.3 and 0.35. Hence, we interpret that the increase in crystallinity leads to an increase in the inter band transition intensity rather than a decrease in the IVCT intensity. The pseudo-direct bandgap energies calculated from Tauc-analysis of heated pure $MA_3Bi_2Br_9$ was maintained at the value of E_g = 2.69 eV, as shown in Figure 3 and Table 1. The greater intensity of the interband transition in the annealed samples allowed Tauc band gaps to be determined even in the presence of IVCT. As shown in Table 1, the band gaps appeared unchanged within error in the Sn doped material.

Table 1 Nominal and measured (XPS) percentage of Sn in $MA_3(Sn_xBi_{(1-x)})_2Br_9$ prepared by **(1)** simple room temperature doping and **(2)** room temperature doping followed by 200 °C heating, calculated from XPS core-level spectra, with corresponding bandgap energies calculated from the Tauc-analysis.

Theoretical Sn concentration	Measured Sn concentration (XPS)		Optical Bandgap energy (eV)	
	room temperature	after annealing 200 °C	room temperature	after annealing 200 °C
0%	0%	0%	2.63	2.69
1%	7.02%	2.96 %	-	2.68
25%	31.05%	23.38%	-	2.69
30%	38.63%	36.00%	-	2.66
35%	34.37%	36.86%	-	2.69
40%	31.02%	42.09%	-	2.69
50%	51.58%	47.80%	-	2.68
60%	60.62%	60.27%	2.65	2.69

The same investigations of mixed-valent Sn doping were carried out on the iodide analogue: $MA_3Bi_2I_9$ to determine if mechanochemical synthesis is able to produce mixed valence doping in iodides. The Sn-doped $MA_3(Sn_xBi_{(1-x)})_2I_9$ samples were prepared by room temperature mechanochemical reaction in air where x = 0, 0.2, 0.3, 0.4, 0.5. Half of each sample was heated at 200 °C in the furnace in air for two hours to increase the crystallinity of as-made doped materials. No obvious colour change for both room temperature prepared and 200 °C heated $MA_3(Sn_xBi_{(1-x)})_2I_9$ (Figure S3). By increasing the doping level of Sn, same as its bromide, no change in lattice parameter were observed by powder XRDError! Reference source not found.**,** and the peak width slightly increased from low to high Sn-content (Figure S4). The intensity of impurity peaks for starting material SnI_2 was increased in powder XRD patterns in high Sn-containing samples, and no signal of by-product BiOI was displayed. All results show the intended Sn doping was unsuccessful for the iodide analogue. Consistent with the sample colour, the UV-Vis absorption spectra for both room temperature and heated $MA_3(Sn_xBi_{(1-x)})_2I_9$ shown no significant change compared to undoped $MA_3Bi_2I_9$ as shown in, and the direct bandgap energies calculated from Tauc-analysis remained unchanged (Figure S5, S6).

One of the reasons for the failure of mixed-valent Sn doping into $MA_3Bi_2I_9$ may come from the structural difference between $MA_3Bi_2Br_9$. Compared to 2D layered material $MA_3Bi_2Br_9$, which has a trigonal crystal structure with the space group *P-3m1* crystal structure, the positions of Bi atoms in the 0D $MA_3Bi_2I_9$ lattice possesses monoclinic crystal structure with the space group *C12/c1* were different. Alternatively, there may be important chemical differences between I and Br which prevent Sn doping into its iodide. Further investigation on theoretical calculations using density functional theory (DFT) can be done to reveal reasons in electronic aspects.

Conclusion

We report a method that overcomes the high bandgap energy of the 2D layered bismuth solar absorber, $MA_3Bi_2Br_9$, which may highly increase the power conversion efficiency (PCE) in its PV application. We have increased the visible and NIR light absorbance (450 to 800 nm) of $MA_3Bi_2Br_9$ *via* ambient mechanochemical doping reactions of $SnBr_2$ in air. A spontaneous colour change from bright yellow to black was observed during the reaction. We noted that the optimised optical performance of Sn-doped $MA_3(Sn_xBi_{(1-x)})_2Br_9$ are obtained when x = 0.3 and 0.35, which both appear black. We elucidate this enhancement to mixed-valence doping of Sn(II) and Sn(IV) oxidation state on the Bi site, which introduces the intervalence charge transfer (IVCT) into our pure phase $MA_3Bi_2Br_9$. The IVCT process provides an additional energy transition in the visible and NIR regions, resulting in a significant improvement in light absorbance. Powder X-ray diffraction (PXRD) shows no secondary phases for $MA_3(Sn_xBi_{(1-x)})_2Br_9$ including x = 0, even after heating at 200°C to induce crystallisation and homogeneity. X-ray photoelectron spectroscopy (XPS) suggests the presence of Sn(II) and Sn(IV) oxidation states. Our Sn-doped $MA_3(Sn_xBi_{(1-x)})_2Br_9$ is air-stable for extended periods. In contrast, attempts to dope Sn into $MA_3Bi_2I_9$, appear not to give a mixed valence product.

Conflicts of Interest

There are no conflicts to declare

Acknowledgements

The authors thank Chantalle Krajewska for helpful discussions.

References

1. A. Kojima, K. Teshima, Y. Shirai and T. Miyasaka, *J. Am. Chem. Soc.*, 2009, **131**, 6050-6051.
2. M. M. Lee, J. Teuscher, T. Miyasaka, T. N. Murakami and H. J. Snaith, *SCIENCE*, 2012, **338**, 643-647.
3. H. J. Snaith, *The Journal of Physical Chemistry Letters*, 2013, **4**, 3623-3630.
4. H. S. Jung and N. G. Park, *Small*, 2015, **11**, 10-25.
5. G. P. Nagabhushana, R. Shivaramaiah and A. Navrotsky, *Proc Natl Acad Sci U S A*, 2016, **113**, 7717-7721.
6. W. J. Serfontein and R. Mekel, *Res Commun Chem Pathol Pharmacol*, 1979, **26**, 391-411.
7. A. M. Ganose, C. N. Savory and D. O. Scanlon, *Chemical Communications*, 2017, **53**, 20-44.
8. H. Tsai, W. Nie, J.-C. Blancon, C. C. Stoumpos, R. Asadpour, B. Harutyunyan, A. J. Neukirch, R. Verduzco, J. J. Crochet, S. Tretiak, L. Pedesseau, J. Even, M. A. Alam, G. Gupta, J. Lou, P. M. Ajayan, M. J. Bedzyk, M. G. Kanatzidis and A. D. Mohite, *Nature*, 2016, **536**, 312-316.
9. J.-W. Lee, Z. Dai, T.-H. Han, C. Choi, S.-Y. Chang, S.-J. Lee, N. De Marco, H. Zhao, P. Sun, Y. Huang and Y. Yang, *Nature Communications*, 2018, **9**, 3021.
10. I. C. Smith, E. T. Hoke, D. Solis-Ibarra, M. D. McGehee and H. I. Karunadasa, *Angewandte Chemie International Edition*, 2014, **53**, 11232-11235.
11. D. B. Mitzi, *Journal of the Chemical Society, Dalton Transactions*, 2001, DOI: 10.1039/B007070J, 1-12.
12. J. S. Manser, J. A. Christians and P. V. Kamat, *Chem. Rev.*, 2016, **116**, 12956-13008.
13. R. E. Brandt, V. Stevanović, D. S. Ginley and T. Buonassisi, *MRS Communications*, 2015, **5**, 265-275.
14. Y. Shen, J. Yin, B. Cai, Z. Wang, Y. Dong, X. Xu and H. Zeng, *Nanoscale Horizons*, 2020, **5**, 580-585.
15. K. K. Bass, L. Estergreen, C. N. Savory, J. Buckeridge, D. O. Scanlon, P. I. Djurovich, S. E. Bradforth, M. E. Thompson and B. C. Melot, *Inorganic Chemistry*, 2017, **56**, 42-45.
16. T. L. Hodgkins, C. N. Savory, K. K. Bass, B. L. Seckman, D. O. Scanlon, P. I. Djurovich, M. E. Thompson and B. C. Melot, *Chemical Communications*, 2019, **55**, 3164-3167.
17. D. Phuyal, S. M. Jain, B. Philippe, M. B. Johansson, M. Pazoki, J. Kullgren, K. O. Kvashnina, M. Klintenberg, E. M. J. Johansson, S. M. Butorin, O. Karis and H. Rensmo, *Journal of Materials Chemistry A*, 2018, **6**, 9498-9505.
18. M. Roy, S. Ghorui, Bhawna, J. Kangsabanik, R. Yadav, A. Alam and M. Aslam, *The Journal of Physical Chemistry C*, 2020, **124**, 19484-19491.
19. M. Leng, Z. Chen, Y. Yang, Z. Li, K. Zeng, K. Li, G. Niu, Y. He, Q. Zhou and J. Tang, 2016, **55**, 15012-15016.
20. J. W. Verhoeven, *Pure and Applied Chemistry*, 1996, **68**, 2223-2286.
21. K. Prassides, P. Day and A. K. Cheetham, *J. Am. Chem. Soc.*, 1983, **105**, 3366-3368.
22. Alkhatib, II, C. Garlisi, M. Pagliaro, K. Al-Ali and G. Palmisano, *Catal. Today*, 2020, **340**, 209-224.
23. D. Chong, X. Wan and J. Zhang, *J. Mater. Chem. C*, 2017, **5**, 6442-6449.
24. C. J. Krajewska, R. Palgrave, S. R. Kavanagh, L. Zhang, D. J. Kubicki, D. O. Scanlon, K. Dey, K. Galkowski, C. P. Grey, S. D. Stranks and A. Walsh, *Chemical Science*, 2021, DOI: 10.1039/D1SC03775G.
25. D. A. Davis, A. Hamilton, J. L. Yang, L. D. Cremar, D. Van Gough, S. L. Potisek, M. T. Ong, P. V. Braun, T. J. Martinez, S. R. White, J. S. Moore and N. R. Sottos, *NATURE*, 2009, **459**, 68-72.
26. S. Kumar, S. Jain, M. Nehra, N. Dilbaghi, G. Marrazza and K. H. Kim, *COORDINATION CHEMISTRY REVIEWS*, 2020, **420**.
27. X. L. Li, C. Q. Yang, B. Sun, S. L. Cai, Z. M. Chen, Y. Q. Lv, J. Zhang and Y. Liu, *JOURNAL OF MATERIALS CHEMISTRY A*, 2020, **8**, 16045-16060.

28. C. A. López, C. Abia, J. Gainza, P. Kayser, N. N. Nemes, O. J. Dura, J. L. Martínez, M. T. Fernández-Díaz, C. Álvarez-Galván and J. A. Alonso, *Materials Advances*, 2021, **2**, 3620-3628.
29. T. Friscic, C. Mottillo and H. M. Titi, *ANGEWANDTE CHEMIE-INTERNATIONAL EDITION*, 2020, **59**, 1018-1029.
30. S. L. James, C. J. Adams, C. Bolm, D. Braga, P. Collier, T. Friscic, F. Grepioni, K. D. M. Harris, G. Hyett, W. Jones, A. Krebs, J. Mack, L. Maini, A. G. Orpen, I. P. Parkin, W. C. Shearouse, J. W. Steed and D. C. Waddell, *CHEMICAL SOCIETY REVIEWS*, 2012, **41**, 413-447.
31. H. Ishihara, K. Watanabe, A. Iwata, K. Yamada, Y. Kinoshita, T. Okuda, V. G. Krishnan, S. Q. Dou and A. Weiss, *Zeitschrift Fur Naturforschung Section a-a Journal of Physical Sciences*, 1992, **47**, 65-74.
32. G. Greczynski and L. Hultman, *Scientific Reports*, 2021, **11**, 11195.
33. G. Greczynski and L. Hultman, *Progress in Materials Science*, 2020, **107**, 100591.
34. M. M. S. Karim, A. M. Ganose, L. Pieters, W. W. Winnie Leung, J. Wade, L. Zhang, D. O. Scanlon and R. G. Palgrave, *Chemistry of Materials*, 2019, **31**, 9430-9444.
35. P. Makuła, M. Pacia and W. Macyk, *The Journal of Physical Chemistry Letters*, 2018, **9**, 6814-6817.
36. Q. Li, L. Yin, Z. Chen, K. Deng, S. Luo, B. Zou, Z. Wang, J. Tang and Z. Quan, *Inorganic Chemistry*, 2019, **58**, 1621-1626.